Mechanism of electron conduction in self-assembled alkanethiol monolayer devices

Wenyong Wang, Takhee Lee, and M. A. Reed*
Departments of Electrical Engineering, Applied Physics, and Physics, Yale University, P.O. Box 208284, New Haven, Connecticut 06520, USA

(Received 3 September 2002; revised manuscript received 12 May 2003; published 17 July 2003)

Electron tunneling through self-assembled monolayers (SAM's) of alkanethiols is investigated using nanometer-scale devices. Temperature-dependent current-voltage measurements are performed on alkanethiol SAM's to distinguish between different conduction mechanisms. Temperature-independent electron transport is observed, proving that tunneling is the dominant conduction mechanism of alkanethiols, as well as exhibiting an exponential dependence of tunneling current on the molecule length with a decay coefficient β. From the bias dependence of β, a barrier height Φ_B of 1.39 ± 0.01 eV and a zero-field decay coefficient β_0 of 0.79 ± 0.01 Å^{-1} are determined for alkanethiols.

DOI: 10.1103/PhysRevB.68.035416 PACS number(s): 73.50.−h, 73.61.Ph, 73.40.Gk, 85.65.+h

I. INTRODUCTION

Understanding the transport mechanism in organic molecular layers has gained particular interest recently due to their potential applications in nanometer-scale electronic systems.[1–5] One of the molecular systems that have been studied extensively is alkanethiol $[CH_3(CH_2)_{n-1}SH]$ because it forms a robust self-assembled monolayer (SAM) on Au surfaces.[6] A few groups have utilized scanning tunneling microscope,[7] conducting atomic force microscope,[8,9] or mercury-drop junctions[10] to investigate electron transport through alkanethiols at room temperature and claimed that the transport mechanism is tunneling. Although the electron conduction is expected to be tunneling when the Fermi levels of contacts lie within the highest occupied molecular orbital and lowest unoccupied molecular orbital (HOMO-LUMO) gap of a short-length molecule as for the case of these alkanethiols,[11] in the absence of temperature-dependent current-voltage $[I(V,T)]$ characteristics such a claim is unsubstantiated since other conduction mechanisms (such as thermionic or hopping conduction) can contribute and complicate the analysis.

In this study, electron transport through alkanethiol self-assembled monolayers is investigated using a device structure that enables $I(V,T)$ measurements. The measured $I(V)$ data are compared with theoretical calculations. $I(V)$ measurements on various alkanethiols of different molecular lengths are also performed for the study of length-dependent conduction behavior.

II. EXPERIMENT

Electronic transport measurements on alkanethiol SAM's were performed using a device structure similar to one reported previously.[2,12] In this device, as illustrated in Fig. 1, a number of molecules (~several thousands) are sandwiched between two metallic contacts. This technique provides a stable device structure and makes cryogenic measurements possible. The device fabrication starts with a high-resistivity silicon wafer with low-stress Si_3N_4 film deposited on both sides by low-pressure chemical vapor deposition (LPCVD). By standard photolithography processing, a suspended Si_3N_4 membrane (size of 40 μm×40 μm and thickness of ~70 nm) is fabricated on the topside of the wafer. Subsequent *e*-beam lithography and reactive ion etching create a single pore with a diameter of tens of nanometers through the membrane. As the next step, 150 nm gold is thermally evaporated onto the topside of the wafer to fill the pore and form one of the metallic contacts. The device is then transferred into a molecular solution to deposit the SAM layer. For our experiments, a ~5 mM alkanethiol solution is prepared by adding ~10 μL alkanethiols into 10 mL ethanol. The deposition is done in solution for 24 h inside a nitrogen-filled glovebox with an oxygen level of less than 100 ppm. Three molecules

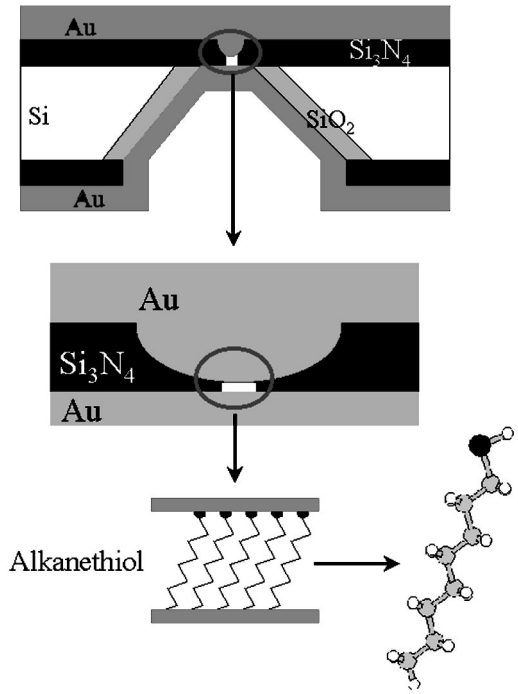

FIG. 1. Schematics of a nanometer-scale device used in this study. Top schematic is the cross section of a silicon wafer with a nanometer-scale pore etched through a suspended silicon nitride membrane. Middle and bottom schematics show a Au-SAM-Au junction formed in the pore area. The structure of octanethiol is shown as an example.

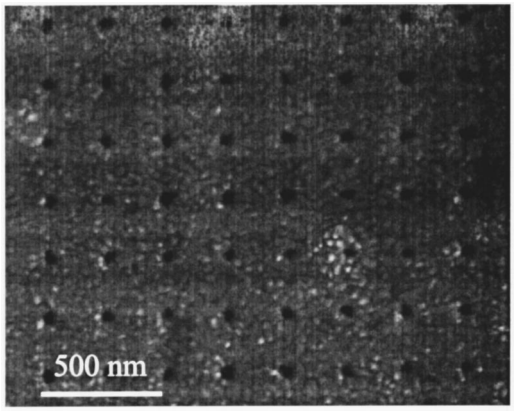

FIG. 2. Scanning electron microscope image of a representative array of pores used to calibrate device size. The scale bar is 500 nm.

of different molecular lengths—octanethiol $[CH_3(CH_2)_7SH$, denoted as C8, for the number of alkyl units], dodecanethiol $[CH_3(CH_2)_{11}SH$, denoted as C12], and hexadecanethiol $[CH_3(CH_2)_{15}SH$, denoted as C16] were used to form the active molecular components. As a representative example, the chemical structure of octanethiol is shown in Fig. 1. In order to statistically determine the pore size, test patterns (arrays of pores) were created under similar fabrication conditions. Figure 2 shows a scanning electron microscope (SEM) image of such test pattern arrays. This indirect measurement of device size is done since SEM examination of the actual device can cause hydrocarbon contamination of the device and subsequent contamination of the monolayer. From regression analysis of 298 pores, the device sizes of the C8, C12, and C16 samples are predicted as 46 ± 2, 45 ± 2, and 45 ± 2 nm in diameters, respectively (99% confidence interval). The sample is then transferred in ambient conditions to an evaporator that has a cooling stage to deposit the opposing Au contact. During the thermal evaporation (under the pressure of $\sim10^{-8}$ Torr), liquid nitrogen is kept flowing through the cooling stage in order to avoid thermal damage to the molecular layer. This technique reduces the kinetic energy of evaporated Au atoms at the surface of the monolayer, thus preventing Au atoms from punching through the monolayer. For the same reason the evaporation rate is kept very low. For the first 10 nm gold evaporated, the rate is less than 0.1 Å/s. Then the rate is increased slowly to 0.5 Å/s for the rest of the evaporation and a total of 200 nm gold is deposited to form the contact. The device is subsequently packaged and loaded into a Janis cryostat. The sample temperature is varied from 300 to 77 K by flowing cryogen vapor onto the sample (and thermometer) using a closed-loop temperature controller. Two-terminal dc $I(V)$ measurements are performed using an HP4145B semiconductor parameter analyzer.

III. RESULTS

A. Temperature-dependent current-voltage $[I(V,T)]$ measurement

In Table I, possible conduction mechanisms are listed with their characteristic current, temperature, and voltage dependences.[13,14] Based on whether thermal activation is involved, the conduction mechanisms fall into two distinct categories: (i) thermionic or hopping conduction, which has temperature-dependent $I(V)$ behavior, and (ii) direct tunneling or Fowler-Nordheim tunneling, which does not have temperature-dependent $I(V)$ behavior. For example, thermionic and hopping conductions have been observed for 4-thioacetylbiphenyl SAM's (Ref. 2) and 1,4-phenelyene diisocyanide SAM's (Ref. 15). On the other hand, the conduction mechanism is expected to be tunneling when the Fermi levels of contacts lie within the large HOMO-LOMO gap for short-length molecules, as for the case of the alkyl-chain or Xe-chain molecular system.[11,16] Previous work on Langmuir-Blodgett alkane monolayers[17,18] exhibited a large impurity-dominated transport component, complicating the analysis. $I(V)$ measurements on self-assembled alkanethiol monolayers have also been reported;[7–10,19–21] however, all of these measurements were performed at fixed temperature (300 K), which is insufficient to prove tunneling as the dominant mechanism. Without temperature-dependent current-voltage characterization, other conduction mechanisms (such as thermionic or hopping conduction) cannot be excluded. Reported here are $I(V)$ measurements in a sufficiently wide tempera-

TABLE I. Possible conduction mechanisms (adapted from Ref. 13).

Conduction mechanism	Characteristic behavior	Temperature dependence	Voltage dependence
Direct tunneling[a]	$J\sim V\exp\left(-\frac{2d}{\hbar}\sqrt{2m\Phi}\right)$	none	$J\sim V$
Fowler-Nordheim tunneling	$J\sim V^2\exp\left(-\frac{4d\sqrt{2m}\Phi^{3/2}}{3q\hbar V}\right)$	none	$\ln\left(\frac{J}{V^2}\right)\sim\frac{1}{V}$
Thermionic emission	$J\sim T^2\exp\left(-\frac{\Phi-q\sqrt{qV/4\pi\varepsilon d}}{kT}\right)$	$\ln\left(\frac{J}{T^2}\right)\sim\frac{1}{T}$	$\ln(J)\sim V^{1/2}$
Hopping conduction	$J\sim V\exp\left(-\frac{\Phi}{kT}\right)$	$\ln\left(\frac{J}{V}\right)\sim\frac{1}{T}$	$J\sim V$

[a]This characteristic of direct tunneling is valid for the low-bias regime [see Eq. (3a)].

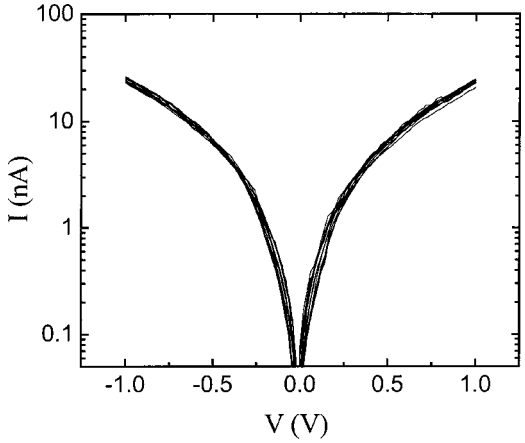

FIG. 3. Temperature-dependent $I(V)$ characteristics of dodecanethiol (C12). $I(V)$ data at temperature from 300 to 80 K with 20 K steps are plotted on a logarithmic scale.

ture range (300–80 K) and resolution (10 K) to determine the mechanism of self-assembled alkanethiol molecular systems.

Figure 3 shows a representative $I(V,T)$ characteristic of dodecanethiol (C12) measured with the device structure as shown in Fig. 1. Positive bias corresponds to electrons injected from the physisorbed Au contact (bottom contact in Fig. 1) into the molecules. By using a contact area of 45 ± 2 nm in diameter, a current density of ~ 1500 ± 200 A/cm^2 at 1.0 V is determined. No significant temperature dependence of the characteristics (from $V=0$ to 1.0 V) is observed over the range from 300 to 80 K. An Arrhenius plot [$\ln(I)$ versus $1/T$] of this is shown in Fig. 4(a), exhibiting little temperature dependence in the slopes of $\ln(I)$ versus $1/T$ at different bias and thus indicating the absence of thermal activation. Therefore, we conclude that the conduction mechanism through alkanethiol is tunneling. The tunneling through alkanethiol SAM's has been assumed as ''through-bond'' tunneling—i.e., along the tilted molecular chains between the metal contacts.[8] Based on the applied bias as compared with the barrier height (Φ_B), the tunneling through a SAM layer can be categorized into either direct ($V<\Phi_B/e$) or Fowler-Nordheim ($V>\Phi_B/e$) through-bond tunneling. These two tunneling mechanisms can be distinguished due to their distinct voltage dependences (see Table I). Analysis of $\ln(I^2/V)$ versus $1/V$ [in Fig. 4(b)] shows no significant voltage dependence, indicating no obvious Fowler-Nordheim transport behavior in this bias range (0 to 1.0 V) and thus determining that the barrier height is larger than the applied bias: i.e., $\Phi_B>1.0$ eV. This study is restricted to applied biases $\leqslant 1.0$ V. The transition from direct to Fowler-Nordheim through-bond tunneling requires higher bias and is under study at present. Having established tunneling as the conduction mechanism, we can now obtain the barrier height by comparing our experimental $I(V)$ data with theoretical calculations from a tunneling model.

B. Tunneling characteristics through alkanethiols

To describe the transport through a molecular system having HOMO and LUMO energy levels, one of the applicable

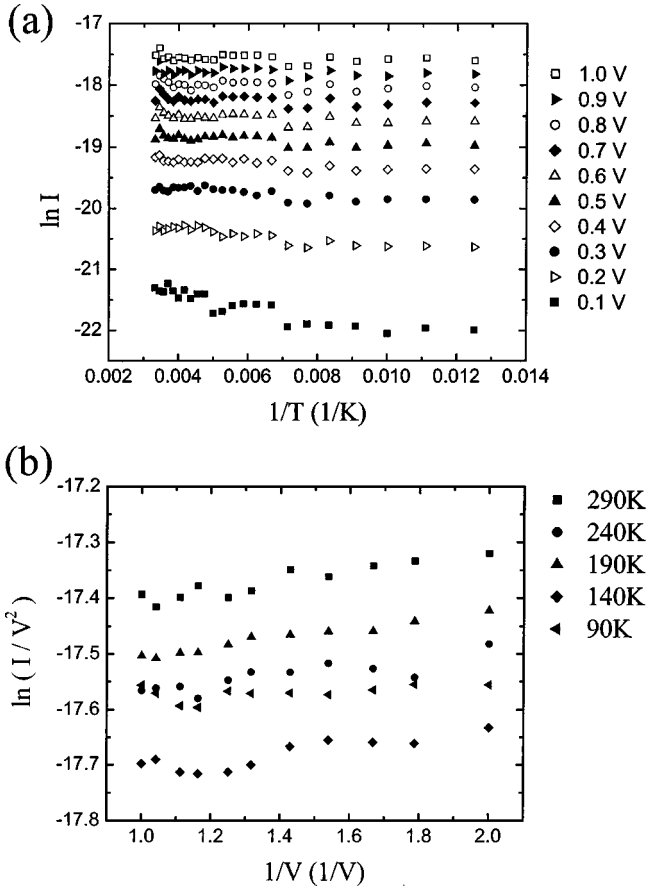

FIG. 4. (a) Arrhenius plot generated from the $I(V)$ data in Fig. 3, at voltages from 0.1 to 1.0 V with 0.1 V steps. (b) Plot of $\ln(I^2/V)$ vs $1/V$ at selected temperatures.

models is the Franz two-band model.[22–25] This model provides a nonparabolic energy-momentum $E(k)$ dispersion relationship by considering the contributions of both the HOMO and LUMO energy levels:[22,23]

$$k^2=\frac{2m^*}{\hbar^2}E\left(1+\frac{E}{E_g}\right), \tag{1}$$

where k is the imaginary part of wave vector of electrons, m^* is the electron effective mass, h $(=2\pi\hbar)$ is Planck's constant, E is the electron energy, and E_g is the HOMO-LUMO energy gap. From this nonparabolic $E(k)$ relationship, the effective mass of the electron tunneling through the SAM can be deduced by knowing the barrier height of the metal-SAM-metal junction.[23]

When the Fermi level of the metal is aligned close enough to one energy level (either HOMO or LUMO), the effect of the other distant energy level on the tunneling transport is negligible, and the widely used Simmons model[26] is an excellent approximation.[27] In the following we use the Simmons model to characterize our experimental $I(V)$ data and later compare it to the Franz model to examine the validity of the approximation.

The Simmons model expresses the tunneling current density through a barrier in the tunneling regime of $V<\Phi_B/e$ as[10,26]

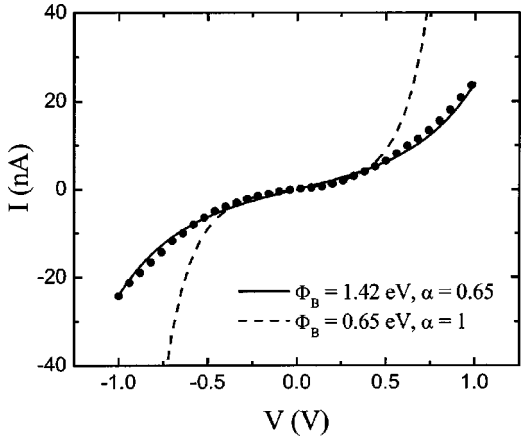

FIG. 5. Measured C12 $I(V)$ data (circular symbols) is compared with calculation (solid curve) using the optimum fitting parameters of $\Phi_B = 1.42$ eV and $\alpha = 0.65$. The calculated $I(V)$ from a simple rectangular model ($\alpha = 1$) with $\Phi_B = 0.65$ eV is also shown as the dashed curve.

$$J = \left(\frac{e}{4\pi^2\hbar d^2}\right)\left\{\left(\Phi_B - \frac{eV}{2}\right) \times \exp\left[-\frac{2(2m)^{1/2}}{\hbar}\alpha\left(\Phi_B - \frac{eV}{2}\right)^{1/2} d\right] - \left(\Phi_B + \frac{eV}{2}\right) \times \exp\left[-\frac{2(2m)^{1/2}}{\hbar}\alpha\left(\Phi_B + \frac{eV}{2}\right)^{1/2} d\right]\right\}, \quad (2)$$

where m is the electron mass, d is the barrier width, Φ_B is the barrier height, V is the applied bias, and α is a unitless adjustable parameter that is introduced to modify the simple rectangular barrier model or to account for an effective mass.[9,10,26] $\alpha = 1$ corresponds to the case of a rectangular barrier and bare electron mass and has been previously shown not to fit $I(V)$ data well for some alkanethiol measurements at fixed temperature (300 K).[10]

From Eq. (2), by adjusting two parameters Φ_B and α, a nonlinear least-squares fitting can be performed to fit the measured C12 $I(V)$ data.[28] By using a device size of 45 nm in diameter, the best fitting parameters (minimized χ^2) for the room-temperature C12 $I(V)$ data were found to be $\Phi_B = 1.42 \pm 0.04$ eV and $\alpha = 0.65 \pm 0.01$ (C12, 300 K), where the error ranges of Φ_B and α are dominated by potential device size fluctuations of 2 nm. A second independently fabricated device with C12 gave values of $\Phi_B = 1.37 \pm 0.03$ eV and $\alpha = 0.66 \pm 0.01$. Likewise, a data set was obtained and fitting was done for hexadecanethiol (C16), which yielded values of $\Phi_B = 1.40 \pm 0.03$ eV and $\alpha = 0.68 \pm 0.01$ (C16, 300 K).

Using $\Phi_B = 1.42$ eV and $\alpha = 0.65$, a calculated $I(V)$ for C12 is plotted as a solid curve in Fig. 5. A calculated $I(V)$ for $\alpha = 1$ and $\Phi_B = 0.65$ eV (which gives the best fit at the low-bias range) is shown as the dashed curve in the same figure, illustrating that with $\alpha = 1$ only limited regions of the $I(V)$ can be fit (specifically here, for $V < 0.3$ V). Although the physical meaning of α is not unambiguously defined, it provides a way of applying the tunneling model of a rectangular barrier to tunneling either through a nonrectangular barrier,[10] a proposed effective mass (m^*) of the tunneling electrons through the molecules[9,23] (i.e., for $\alpha = 0.65$, m^* would be $0.42m$ here), or a combination of both. Note that the $I(V)$ data can be fit to arbitrary accuracy over the entire bias range by allowing a slight bias dependence of α (or Φ_B).

Nonlinear least-squares fittings on C12 $I(V)$ data at all temperatures allow us to determine $\{\Phi_B, \alpha\}$ over the entire temperature range and show that Φ_B and α values are temperature independent in our temperature range (300–80 K). For the first C12 sample reported, a value of $\Phi_B = 1.45 \pm 0.01$ eV and $\alpha = 0.64 \pm 0.01$ was obtained [$1\sigma_M$ (standard error)].

C. Length dependence of tunneling through alkanethiols

Equation (2) can be approximated in two limits: low bias and high bias as compared with the barrier height Φ_B. For the low-bias range, Eq. (2) can be approximated as[26]

$$J \approx \left(\frac{(2m\Phi_B)^{1/2}e^2\alpha}{h^2 d}\right) V \exp\left[-\frac{2(2m)^{1/2}}{\hbar}\alpha(\Phi_B)^{1/2} d\right]. \quad (3a)$$

To determine the high-bias limit, we compare the relative magnitudes of the first and second exponential terms in Eq. (2). At high bias, the first term is dominant and thus the current density can be approximated as

$$J \approx \left(\frac{e}{4\pi^2\hbar d^2}\right)\left\{\left(\Phi_B - \frac{eV}{2}\right) \times \exp\left[-\frac{2(2m)^{1/2}}{\hbar}\alpha\left(\Phi_B - \frac{eV}{2}\right)^{1/2} d\right]\right. \quad (3b)$$

According to the Simmons model, in the low-bias regime the tunneling current is dependent on the barrier width d as $J \propto (1/d)\exp(-\beta_0 d)$, where β_0 is a bias-independent decay coefficient,

$$\beta_0 = \frac{2(2m)^{1/2}}{\hbar}\alpha(\Phi_B)^{1/2}, \quad (4a)$$

while at higher bias, $J \propto (1/d^2)\exp(-\beta_V d)$, where β_V is a bias-dependent decay coefficient,

$$\beta_V = \frac{2(2m)^{1/2}}{\hbar}\alpha\left(\Phi_B - \frac{eV}{2}\right)^{1/2} = \beta_0\left(1 - \frac{eV}{2\Phi_B}\right)^{1/2}. \quad (4b)$$

At high bias β_V decreases as bias increases [Eq. (4b)], which results from the barrier lowering effect due to the applied bias.

We define the high-bias range somewhat arbitrarily by comparing the relative magnitudes of the first and second exponential terms in Eq. (2). Using $\Phi_B = 1.42$ eV and $\alpha = 0.65$ obtained from a nonlinear least-squares fitting of the C12 $I(V)$ data, the second term becomes less than ~10% of the first term at ~0.5 V, which is chosen as the boundary of low- and high-bias ranges.

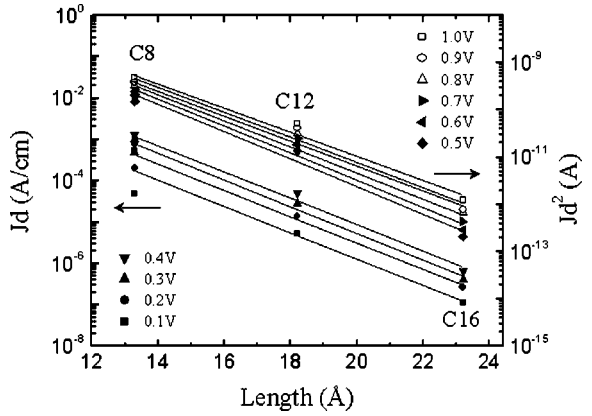

FIG. 6. Log plot of tunneling current densities multiplied by molecular length d at low bias and by d^2 at high bias (symbols) vs molecular lengths. The lines through the data points are linear fittings.

To determine the β values for alkanethiols used in this study, three alkanethiols of different molecular lengths—octanethiol (C8), dodecanethiol (C12), and hexadecanethiol (C16)—were investigated to generate length-dependent $I(V)$ data. Figure 6 is a logarithmic plot of tunneling current densities multiplied by molecular length (Jd at low bias and Jd^2 at high bias) as a function of the molecular length for these alkanethiols.[29] The molecular lengths used in this plot are 13.3, 18.2, and 23.2 Å for C8, C12, and C16, respectively (each molecular length was determined by adding an Au-thiol bonding length to the length of molecule[8]). Note that these lengths assume through-bond tunneling.[8]

As seen in Fig. 6, the tunneling current shows an exponential dependence on molecular length. The β values can be determined from the slope at each bias and are plotted in Fig. 7. The error bar of an individual β value in this plot was obtained by considering both the device size uncertainties and the linear fitting errors.

According to Eq. (4b), β_V^2 depends on bias V linearly in the high bias range. The inset in Fig. 7 is a plot of β_V^2 versus

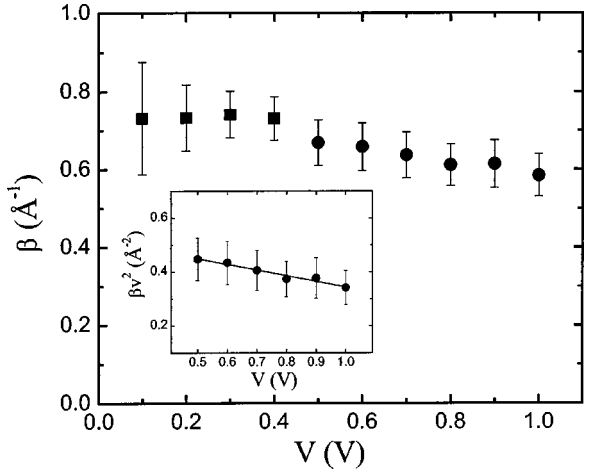

FIG. 7. Plot of β vs bias in the low-bias range (square symbols) and high-bias ranges (circular symbols). The inset shows a plot of β_V^2 vs bias with a linear fitting.

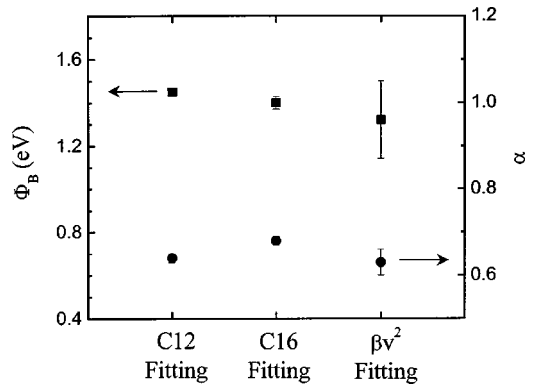

FIG. 8. Summary of Φ_B (square symbols) and α (circular symbols) values obtained from alkanethiol $I(V)$ fittings and the β_V^2-V fitting.

V in this range (0.5–1.0 V) along with a linear fitting of the data. From this fitting, $\Phi_B = 1.32 \pm 0.18$ eV and $\alpha = 0.63 \pm 0.03$ were obtained from the intercept and slope, respectively, consistent with the more precise values obtained from the nonlinear least-squares fitting in the previous section. The Φ_B (square symbols) and α (circular symbols) values obtained by the C12 and C16 $I(V)$ data fittings and β_V^2-V linear fitting are summarized in Fig. 8. The combined values are $\Phi_B = 1.39 \pm 0.01$ eV $(1\sigma_M)$ and $\alpha = 0.65 \pm 0.01$ $(1\sigma_M)$. Using Eq. (4a), we can derive a zero-field decay coefficient β_0 of 0.79 ± 0.01 Å^{-1}.

β values for alkanethiols obtained by various experimental techniques have previously been reported.[7–10,19–21] In order to compare with these reported β values, we also performed a length-dependent analysis on our experimental data according to the generally used equation[7–11,30]

$$G = G_0 \exp(-\beta d). \tag{5}$$

This gives a β value from 0.83 to 0.72 Å^{-1} in the bias range from 0.1 to 1.0 V, which is comparable to results reported previously; for example, Holmlin *et al.* reported a β value of 0.87 Å^{-1} by mercury-drop experiments,[10] and Wold *et al.* have reported a β of 0.94 Å^{-1} and Cui *et al.* reported a β of 0.6 Å^{-1} for various alkanethiols by using a conducting atomic force microscope technique.[8,9] These reported β were treated as bias-independent quantities, contrary to the results reported here and that observed in a slightly different alkane system (ligand-encapsulated nanoparticle/alkane-dithiol molecules).[31]

D. Franz model

We have analyzed our experimental data using a Franz two-band model.[22,24,25] Since there is no reliable experimental data on the Fermi level alignment in these metal-SAM-metal systems, Φ_B and m^* are treated as adjustable parameters. We performed a least-squares fit on our data with the Franz nonparabolic $E(k)$ relationship [Eq. (1)] using an alkanethiol HOMO-LUMO gap of 8 eV.[32,33] Figure 9 shows the resultant $E(k)$ relationship[23] and the corresponding energy band diagrams. The zero of energy in this plot was chosen as the LUMO energy. The best fitting parameters ob-

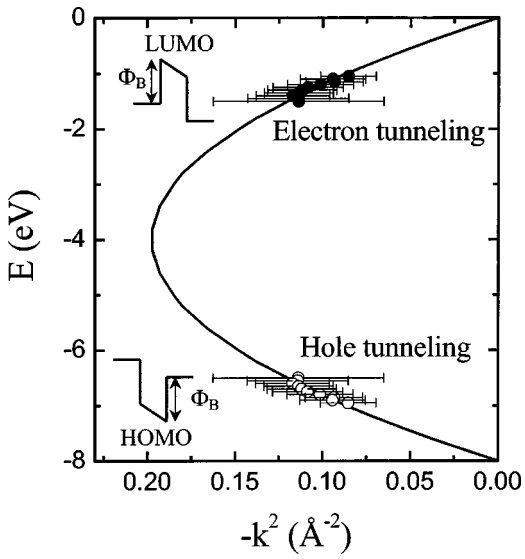

FIG. 9. $E(k)$ relationship (symbols) generated from the length-dependent measurement data for alkanethiols. Solid and open symbols correspond to electron and hole tunneling, respectively. The insets show the corresponding energy band diagrams. The solid curve is the Franz two-band expression for $m^*=0.38m$.

tained by minimizing χ^2 were $\Phi_B=1.55\pm0.59$ eV and $m^*=(0.38\pm0.20)m$, where the error ranges of Φ_B and m^* are dominated by the error fluctuations of β $[-k^2=(\beta/2)^2]$. Both electron tunneling near the LUMO and hole tunneling near the HOMO can be described by these parameters. $\Phi_B=1.55$ eV indicates that the Fermi level is aligned close to one energy level in either case: therefore, the Simmons model is a valid approximation. The previous best fits obtained from the Simmons model of $\Phi_B=1.39$ eV and $\alpha=0.65$ (corresponding to $m^*=0.42m$ for the rectangular barrier case) are in reasonable agreement.

IV. CONCLUSION

From temperature-dependent current-voltage measurements, tunneling is unambiguously shown to be the dominant transport mechanism in alkanemonothiol SAM's (for $V<\Phi_B/e$), with a barrier height $\Phi_B=1.39\pm0.01$ eV and a nonideal barrier factor $\alpha=0.65\pm0.01$. Exponential length dependence is observed with a bias-dependent decay coefficient (contrary to previous results) with a zero-field decay coefficient β_0 of 0.79 ± 0.01 Å^{-1}.

ACKNOWLEDGMENTS

One of the authors (W.W.) would like to thank R. Panepucci at Cornell University for help and discussions on the device fabrications. We thank A. Barron, M. de Jong, C. Joachim, M. Kamdar, J. Klemic, I. Kretzschmar, X. Li, G. Martin, R. Munden, J. Su, and J. Zhang for helpful discussions and suggestions. This work was supported by DARPA/ONR (Grant No. N00014-01-1-0657), ARO (Grant No. DAAD 19-01-1-0592), AFOSR (Grant No. 17496200110358), and NSF (Grant No. DMR-0095215). The fabrication was performed in part at the Cornell Nano-Scale Science & Technology Facility.

*Author to whom correspondence should be addressed. Electronic address: mark.reed@yale.edu

[1] R. M. Metzger, B. Chen, U. Holpfner, M. V. Lakshmikantham, D. Vuillaume, T. Kawai, X. Wu, H. Tachibana, T. V. Hughes, H. Sakurai, J. W. Baldwin, C. Hosch, M. P. Cava, L. Brehmer, and G. J. Ashwell, J. Am. Chem. Soc. **119**, 10 455 (1997).

[2] C. Zhou, M. R. Deshpande, M. A. Reed, L. Jones II, and J. M. Tour, Appl. Phys. Lett. **71**, 611 (1997).

[3] J. Chen, M. A. Reed, A. M. Rawlett, and J. M. Tour, Science **286**, 1550 (1999); J. Chen, W. Wang, M. A. Reed, A. M. Rawlett, D. W. Price, and J. M. Tour, Appl. Phys. Lett. **77**, 1224 (2000).

[4] C. P. Collier, G. Mattersteig, E. W. Wong, Y. Luo, K. Beverly, J. Sampaio, F. M. Raymo, J. F. Stoddart, and J. R. Heath, Science **289**, 1172 (2000).

[5] M. A. Reed, J. Chen, A. M. Rawlett, D. W. Price, and J. M. Tour, Appl. Phys. Lett. **78**, 3735 (2001).

[6] A. Ulman, *An Introduction to Ultrathin Organic Films from Langmuir-Blodgett to Self-Assembly* (Academic, Boston, 1991).

[7] L. A. Bumm, J. J. Arnold, T. D. Dunbar, D. L. Allara, and P. S. Weiss, J. Phys. Chem. B **103**, 8122 (1999).

[8] D. J. Wold, R. Haag, M. A. Rampi, and C. D. Frisbie, J. Phys. Chem. B **106**, 2813 (2002).

[9] X. D. Cui, X. Zarate, J. Tomfohr, O. F. Sankey, A. Primak, A. L. Moore, T. A. Moore, D. Gust, G. Harris, and S. M. Lindsay, Nanotechnology **13**, 5 (2002).

[10] R. Holmlin, R. Haag, M. L. Chabinyc, R. F. Ismagilov, A. E. Cohen, A. Terfort, M. A. Rampi, and G. M. Whitesides, J. Am. Chem. Soc. **123**, 5075 (2001); M. A. Rampi and G. M. Whitesides, Chem. Phys. **281**, 373 (2002).

[11] M. A. Ratner, B. Davis, M. Kemp, V. Mujica, A. Roitberg, and S. Yaliraki, in *Molecular Electronics: Science and Technology*, The Annals of the New York Academy of Sciences, Vol. 852, edited by A. Aviram and M. Ratner (The New York Academy of Sciences, New York, 1998).

[12] K. S. Ralls, R. A. Buhrman, and R. C. Tiberio, Appl. Phys. Lett. **55**, 2459 (1989).

[13] S. M. Sze, *Physics of Semiconductor Devices*, 2nd ed. (Wiley, New York, 1981).

[14] The models listed in Table I apply to solid-state insulators with one band.

[15] J. Chen, L. C. Calvet, M. A. Reed, D. W. Carr, D. S. Grubisha, and D. W. Bennett, Chem. Phys. Lett. **313**, 741 (1999).

[16] L. Pizzagalli, C. Joachim, X. Bouju, and Ch. Girard, Europhys. Lett. **38**, 97 (1997).

[17] B. Mann and H. Kuhn, J. Appl. Phys. **42**, 4398 (1971).

[18] E. E. Polymeropoulos and J. Sagiv, J. Chem. Phys. **69**, 1836 (1978).

[19] F. F. Fan, J. Yang, L. Cai, D. W. Price, S. M. Dirk, D. V. Kosynkin, Y. Yao, A. M. Rawlett, J. M. Tour, and A. J. Bard, J. Am. Chem. Soc. **124**, 5550 (2002).

[20] K. Slowinski, H. K. Y. Fong, and M. Majda, J. Am. Chem. Soc. **121**, 7257 (1999).

[21] J. F. Smalley, S. W. Feldberg, C. E. D. Chidsey, M. R. Linford, M. D. Newton, and Y. Liu, J. Phys. Chem. **99**, 13 141 (1995).

[22] W. Franz, in *Handbuch der Physik*, edited by S. Flugge (Springer-Verlag, Berlin, 1956), Vol. 17, p. 155.
[23] C. Joachim and M. Magoga, Chem. Phys. **281**, 347 (2002).
[24] G. Lewicki and C. A. Mead, Phys. Rev. Lett. **16**, 939 (1966); R. Stratton, G. Lewicki, and C. A. Mead, J. Phys. Chem. Solids **27**, 1599 (1966); G. H. Parker and C. A. Mead, Phys. Rev. Lett. **21**, 605 (1968).
[25] B. Brar, G. D. Wilk, and A. C. Seabaugh, Appl. Phys. Lett. **69**, 2728 (1996).
[26] J. G. Simmons, J. Appl. Phys. **34**, 1793 (1963).
[27] J. G. Simmons, J. Phys. D **4**, 613 (1971); J. Maserjian and G. P. Petersson, Appl. Phys. Lett. **25**, 50 (1974).
[28] Nonlinear least-squares fittings were performed using MICROCAL ORIGIN 6.0.
[29] Both bias values were used for the C8 data to compensate for an observed asymmetry and are plotted in Fig. 6.
[30] M. P. Samanta, W. Tian, S. Datta, J. I. Henderson, and C. P. Kubiak, Phys. Rev. B **53**, 7626 (1996).
[31] X. D. Cui, A. Primak, X. Zarate, J. Tomfohr, O. F. Sankey, A. L. Moore, T. A. Moore, D. Gust, L. A. Nagahara, and S. M. Lindsay, J. Phys. Chem. B **106**, 8609 (2002).
[32] Although the HOMO-LUMO gap of alkyl-chain-type molecules has been reported (see Ref. 33), there is no experimental data on the HOMO-LUMO gap for the Au/alkanethiol SAM/Au system. 8 eV is commonly used as the HOMO-LUMO gap of alkanethiol.
[33] C. Boulas, J. V. Davidovits, F. Rondelez, and D. Vuillaume, Phys. Rev. Lett. **76**, 4797 (1996); M. Fujihira and H. Inokuchi, Chem. Phys. Lett. **17**, 554 (1972); S. G. Lias, J. E. Bartmess, J. F. Liebman, J. L. Holmes, R. D. Levin, and W. G. Mallard, J. Phys. Chem. Ref. Data Suppl. **17**, 24 (1988).